Geophysical Research Letters

RESEARCH LETTER
10.1029/2024GL109499

Climate Conundrum: A Wet or Dry European and Northern African Climate During the Middle Miocene

R. P. Acosta[1], N. J. Burls[1], M. J. Pound[2], C. D. Bradshaw[3,4], J. McCoy[2], M. Gibson[5], J. M. K. O'Keefe[6], and S. J. Feakins[7]

[1]Department of Atmospheric, Ocean and Earth Sciences, Center for Ocean-Land Atmosphere Studies, George Mason University, Fairfax, VA, USA, [2]Department of Geography and Environmental Sciences, Northumbria University, Newcastle, UK, [3]The Global Systems Institute, University of Exeter, Exeter, UK, [4]Met Office Hadley Centre, Exeter, UK, [5]PetroStrat Ltd, Conwy, UK, [6]Department of Engineering Sciences, Morehead State University, Morehead, KY, USA, [7]Department of Earth Science, University of Southern California, Los Angeles, CA, USA

Key Points:

- Middle Miocene Europe rainfall discrepancy between herpetological (dry) and paleobotanical (wet) records complicate climate model validation
- Simulations that produce dry environments also produce cool North Atlantic sea surface temperatures which are inconsistent with proxies
- SSTs informed by North Atlantic proxies produce wetter environments consistent with paleobotanical evidence

Supporting Information:

Supporting Information may be found in the online version of this article.

Correspondence to:

R. P. Acosta,
racosta6@gmu.edu

Citation:

Acosta, R. P., Burls, N. J., Pound, M. J., Bradshaw, C. D., McCoy, J., Gibson, M., et al. (2024). Climate conundrum: A wet or dry European and Northern African climate during the middle Miocene. *Geophysical Research Letters*, *51*, e2024GL109499. https://doi.org/10.1029/2024GL109499

Received 27 MAR 2024
Accepted 9 OCT 2024

Author Contributions:

Conceptualization: R. P. Acosta, N. J. Burls
Data curation: M. J. Pound, J. McCoy, J. M. K. O'Keefe
Formal analysis: R. P. Acosta
Funding acquisition: R. P. Acosta, N. J. Burls, S. J. Feakins
Investigation: R. P. Acosta
Methodology: R. P. Acosta, M. J. Pound, C. D. Bradshaw
Project administration: R. P. Acosta, N. J. Burls
Resources: R. P. Acosta
Supervision: N. J. Burls, S. J. Feakins

Abstract End of 21st-century hydroclimate projections suggest an expansion of subtropical dry zones, with Mediterranean and Sahel regions becoming much drier. However, paleobotanical assemblage evidence from the middle Miocene (17-12 Ma), suggests both regions were instead humid environments. Here we show that by modifying regional sea surface temperatures (SST) in an Earth System Model (CESM1.2) simulation of the middle Miocene, the increased ocean evaporation and integrated water vapor flux overrides any drying effects associated with warming-induced land-surface evaporation driven by atmospheric CO_2 concentrations. These modifications markedly reduce the bias in the model-data comparison for this period. A vegetation model (BIOME4) forced with simulated climatologies predicts both regions were dominated by mixed forest, which is largely consistent with the paleobotanical record. This study unveils the potential for wetter subtropical Mediterranean climates associated with warming, presenting an alternative scenario from future drying projections with localized SST warming governing regional climate change.

Plain Language Summary Climate models project drier conditions over Europe and Northern Africa due to global warming. However, evidence from a past warm climate period, the middle Miocene (~15 million years ago), finds wetter rather than drier environments. We refine climate model boundary conditions by reconstructing warmer ocean waters in the North Atlantic based on proxy evidence. The warmer ocean produces wetter environments by enhancing North Atlantic precipitation events and the North African monsoon. The increased rainfall and surface temperature cause a vegetation model to predict more forest coverage over Europe and Northern Africa, which is consistent with fossil evidence from ~15 million years ago. This study unveils the potential for wetter climates associated with warming, presenting an alternative scenario from future drying projections, with localized sea surface warming governing regional climate.

1. Introduction

The Miocene Climatic Optimum (MCO), 16.75–14.5 million years ago was a period of peak global warmth during the Miocene (23.1–5.3 Ma) (Foster et al., 2012; Sosdian et al., 2020; Westerhold et al., 2020) with peak atmospheric paleoCO_2 as high as 600–1,100 ppmv (Sosdian et al., 2020; Rae et al., 2021). The MCO represents the lower global mean surface temperature (GMST) range of the projected end of the 23rd-century climate under Shared Socio-economic Pathways (SSPs) 5–8.5, with GMST of 5–10°C above modern-day (Gulev & Thorne, 2021). The MCO is potentially a relevant analog of the Earth system as we consider its future climate. Drying trends are projected to increase in the Mediterranean and Sahel regions under warmer climate conditions (Ukkola et al., 2020; Douville et al., 2021). However, recent analysis shows stabilization of regional warm sea surface temperature (SST) patterns can potentially reverse such drying trends (Dittus et al., 2024).

Looking back at the MCO, herpetological records from southern Europe identified similar dry environments with mean annual precipitation (MAP) 300–5,000 mm lower than preindustrial (Böhme et al., 2011; Botsyun et al., 2022). However, middle Miocene palaeobotanical records found across the Mediterranean region, describe warm yet humid (MAP; 800–2,500 mm) rather than dry environments (Bruch et al., 2007; Pound et al., 2012; Botsyun et al., 2022). A number of middle Miocene simulations (Botsyun et al., 2022; Acosta et al., 2023) support drying patterns, especially at much higher CO_2 concentrations (560–850 ppm). Substantial model disagreement is found within Deep-MIP Miocene model intercomparison project Phase 1 (MioMIP1), where recent paleoclimate

Validation: R. P. Acosta, M. J. Pound, C. D. Bradshaw, J. McCoy, J. M. K. O'Keefe, S. J. Feakins
Visualization: R. P. Acosta, C. D. Bradshaw
Writing – original draft: R. P. Acosta, N. J. Burls, C. D. Bradshaw
Writing – review & editing: R. P. Acosta, N. J. Burls, M. J. Pound, C. D. Bradshaw, S. J. Feakins

modeling efforts have identified the Mediterranean region as the source of the largest uncertainty stemming from low model-data and inter-model agreement (Acosta et al., 2023). Climate signals from North African proxy records during the MCO are rare, but prior vegetation studies have also identified paleoclimate conditions that are conducive to tropical rainforest or at least a much more humid environment than the modern-day (Morley, 2011; Zhang et al., 2014). New data from the region could help dispute the discrepancies between palaeobotanical and herpetological records and the low paleoclimate model agreement.

The intensity of the European rainfall (Jackson et al., 2015; Lavers & Villarini, 2015; Payne et al., 2020; Wang et al., 2023) and the North African monsoon (Acosta & Huber, 2020; Geen et al., 2020; Acosta et al., 2022) events are directly linked to the amount of atmospheric column-integrated water-vapor transport (IVTs) and are strongly influenced by changes to the North Atlantic and Mediterranean SST patterns. Biomarker proxies based on the membrane lipids of marine archaea (TEX_{86}) and the energy reserves of specific haptophyte algae ($U^{K'}_{37}$) are commonly used for ocean temperature reconstructions. TEX_{86} and $U^{K'}_{37}$ evidence from North Atlantic (Ocean Drilling Program Sites 608 and 982) shows SST estimates ranged from 22°C to 32°C or 10–15°C warmer than modern estimates during the MCO (Super et al., 2018, 2020). Middle Miocene (~12 Ma) SST reconstructions based on $U^{K'}_{37}$ at high-latitudes (~70°N; site 907) were ~17°C, and reconstructions from the Mediterranean Sea were ~28°C (Herbert et al., 2016). Previous model-data analysis from MioMIP1study (Burls et al., 2021) are unable to reconcile North Atlantic and the Mediterranean-Tethys Sea SSTs even at much higher CO_2 concentrations (560 ppm or higher). The inability for paleoclimate simulations to capture such SST patterns could lead to biases in simulated hydroclimate conditions. Thus, utilizing changes in regional SST patterns and understanding its link to IVT strength can give us insight into European and North African hydroclimate during the middle Miocene.

A previous Miocene modeling study demonstrated that model-data precipitation differences are reduced when simulated SSTs are informed by available proxy data, where using an idealized zonally uniform SST pattern with more similar equator-to-pole temperature gradient as proxies improves mid-to-high latitude precipitation (Herold et al., 2010). However, the impact of implementing North Atlantic SST patterns on Europe and North Africa has largely been unexplored. In this paper, we incorporate the latest published SST reconstructions for Northern Atlantic warmth during the middle Miocene, force an atmospheric general circulation model (AGCM) with these SST reconstructions, and present a middle Miocene model-data comparison focusing on precipitation over central Europe and North Africa. We seek to reconcile hydroclimate signals from paleobotanical and herpetological proxy records and climate model output. We do this by applying idealized, zonal mean, global, and North Atlantic SST distributions in climate model experiments (Figure 1) and provide a systematic assessment of Miocene European and North African rainfall distribution by analyzing changes in land-ocean surface fluxes and IVTs.

2. Methods

2.1. Terrestrial Data

Paleobotanical and herpetological evidence are often preserved in sedimentary archives and carry assemblage or species-specific information about climate, here we focus on extracting information about precipitation and temperature. A wide variety of fossils (including seeds, pollen, spores, flower, leaves, and wood) and paleosol formation were compiled as evidence of MAP. Classical method of extraction of climate signals from botanical fossils was estimated using the coexistence approach for pollen (Utescher et al., 2014) and Climate Leaf Analysis Multivariate Program for plant leaves (Spicer et al., 2021; Gibson et al., 2022). Proxy estimates of MAT and MAP were compiled from previously published paleobotanical studies (Pound et al., 2012; Bradshaw et al., 2015; Burls et al., 2021; Acosta et al., 2023) (Figure 2 diamond symbol). Herpetological records are also used to derive past MAP (Böhme et al., 2006, 2011; Botsyun et al., 2022) by utilizing functional morphology and the nearest living relative approach (Figure 2 triangle symbol). In addition to the previously published records, we incorporate new paleobotanical data sets derived from new Climate Reconstruction SofTware (CREST) and Climate Reconstruction Analysis using Coexistence Likelihood Estimation (CRACLE) methods (Gibson et al., 2022) (Figure 2 circle symbol). The proxy location was reconstructed to ~15 Ma using GPlates (Müller et al., 2018) with plate reconstructions based on Matthews et al. (2016).

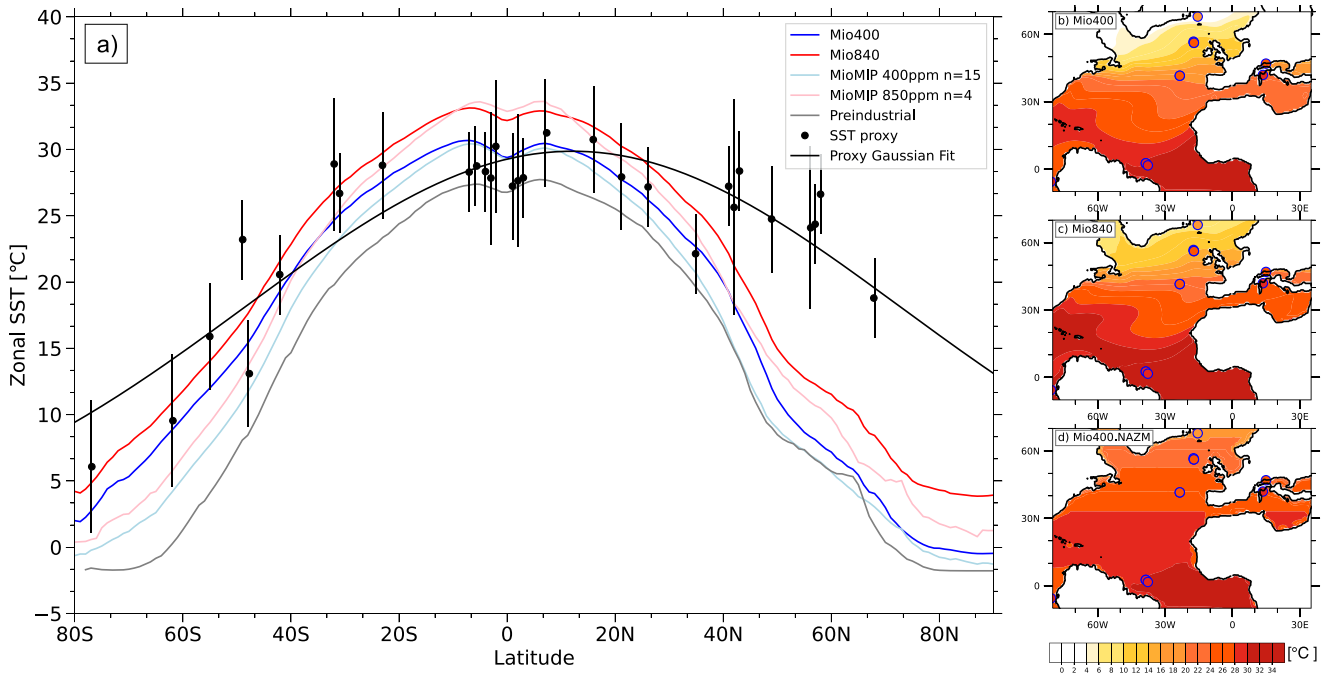

Figure 1. Zonal mean sea surface temperature distribution between MioMIP1, middle Miocene (current study) simulations and proxies (a). The Gaussian curve (black line) derived from proxies was used as the idealized SST distribution in the "NAZM" and "GLZM" experiments (Table S1, Figure S1 in Supporting Information S1). Spatial distribution of North Atlantic SST between the Mio400, Mio840 and Mio400.NAZM simulations, overlain with proxy compilation in circle.

2.2. Climate Simulations and Experimental Designs

We conduct a suit of AGCM simulations (Table S1 in Supporting Information S1) with prescribed SST and sea ice using the National Center for Atmospheric Research, Community Earth System Model version 1.2 (CESM1.2) with Community Atmospheric Model version 5 and Community Land Model 4.5 (Meehl et al., 2013). All simulations were carried out for 24 years with the last 10 years used as the climatology. The simulations used a finite volume dynamical core version of the atmosphere model with a grid spacing of 1.9° × 2.5°. All "Mio"

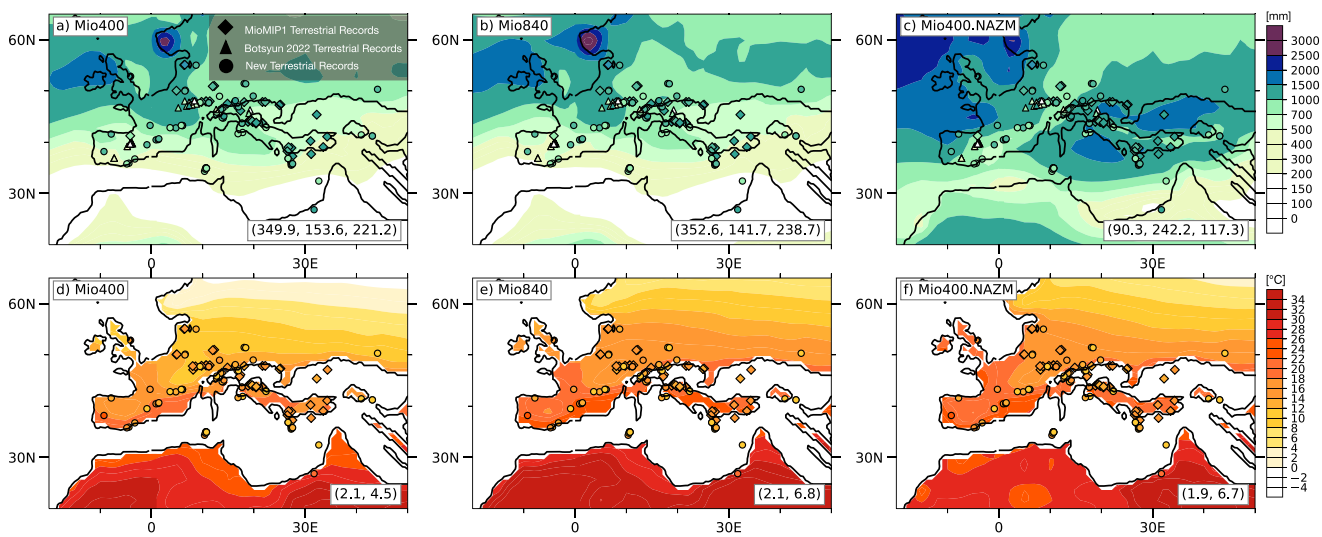

Figure 2. Mean annual precipitation (mm, (a–c)) and mean annual temperature (°C); (d–f) analysis overlain with proxy reconstructions. The MAP RMSB analysis (lower right-hand) shows MioMIP1 paleobotanical, herpetological, and new paleobotanical records. The MAT RMSB analysis (lower right-hand) shows MioMIP1 paleobotanical, and new paleobotanical records.

experiments (Table S1 in Supporting Information S1) use middle Miocene paleogeography, land-ice, and vegetation boundary conditions found in Burls et al. (2021) and Acosta et al. (2022). We provide simulations with a moderate 400 ppm (referred to as "Mio400") and a high 840 ppm (referred to as "Mio840") CO_2 concentration. Prescribed SSTs and sea ice for the middle Miocene Atmosphere General Circulation Model simulations were obtained from previously published (Acosta et al., 2022, 2023; Gaskell et al., 2022) fully coupled (active atmosphere, land, river, ocean, and sea-ice components) CESM1.2 GCM simulations. The fully coupled simulation was previously used for regional monsoon analysis (Acosta et al., 2022), analysis of the global equator-to-pole SST gradient (Gaskell et al., 2022), and incorporated into the MioMIP1 hydrological cycle (Acosta et al., 2023). The global annual mean surface temperature of the 400 and 840 ppm simulations are ∼19°C and ∼22°C, respectively. The global annual mean precipitation of ∼1,280 mm and ∼1,366 mm.

To emulate higher North Atlantic SST patterns described by the proxies, we first perform idealized global zonally uniform SST fields (referred to as "Mio400.GLZM"; Figure S1b in Supporting Information S1) with the annual-mean values derived using a Gaussian curve fitted to the middle Miocene SST estimates found in MioMIP1 (Burls et al., 2021; Figure 1a black curve). We use preindustrial seasonal distribution to construct the zonal monthly mean climatology. For the main body of our analysis, we performed a North Atlantic-focused simulation (referred to as "Mio400.NAZM") where we applied the idealized global zonal SST patterns only over the North Atlantic (0–80°N) while maintaining SST values derived from the Mio400 simulation elsewhere (Figure 1d and Figure S1c in Supporting Information S1).

2.3. Diagnostics (Model-Data Comparison, Moisture Flux, and Vegetation Modeling)

To assess model-data MAP and mean annual temperature (MAT) discrepancy, we use a root-mean-squared error of the bias (referred to here as RMSB) methodology (Bradshaw et al., 2015; Burls et al., 2021; Acosta et al., 2023). The method uses uncertainty overlap to define where model-data values match. The bias is defined as non-overlapping values between the reconstructed and modeled uncertainty ranges, respectively. To provide a conservative error estimate we use the minimum-maximum proxy values as the range of uncertainty. For the models, we use the collocated model grid cell value as the mean and utilize the neighboring grid points as the range of uncertainty. By using the adjacent grid cells we aim to incorporate location uncertainty as it is unreasonable to reconstruct the exact paleoclimate signal at a given paleolocation. Lastly, we then take the regional root-mean-square error of the bias representing the overall discrepancy between the proxies and models.

To provide a framework to measure changes in the European and North African storm tracks, we calculate IVT strength. Although the amount of moisture in the atmosphere does not linearly correlate with the amount of precipitation, IVTs can be used to investigate the thermodynamic (increase in specific humidity q) and dynamic (changes in meridional v and zonal u) response of the atmosphere under differing climate conditions.

$$\mathrm{IVT} = \frac{1}{g}\sqrt{\left(\int_{p_s}^{p} uq\delta p\right)^2 + \left(\int_{p_s}^{p} vq\delta p\right)^2} \tag{1}$$

Equation 1 shows the magnitude of IVT is the sum of zonal moisture transport (uq) and meridional moisture transport (vq) integrated between the upper atmosphere (p) and the surface (p_s). Where g is Earth's gravity, and the p is capped at 300 mb (Lavers & Villarini, 2013, 2015).

To understand changes in paleo-environments under different middle Miocene conditions, we used the vegetation model BIOME4 (Kaplan et al., 2003). BIOME4 is an equilibrium global vegetation model that utilizes a coupled carbon and water flux model to define potential natural biomes according to the bioclimatic ranges and photosynthetic pathways of constituent plant functional types (PFTs). Predictions of the steady-state vegetation distributions are driven by monthly mean precipitation, solar influx (cloud cover), temperature which were derived from the simulations, and prescribed with atmospheric CO_2 concentration and soil properties (Pound et al., 2014; Retallack, 2022) for water holding capacity and percolation rates. BIOME4 has been used in many paleoclimate studies for both past cold and warm climates (e.g., Harrison & Prentice, 2003; Ni & Herzschuh, 2011; Salzmann et al., 2008; Zhao et al., 2011) as well as for the present (Ni & Herzschuh, 2011) and future (Zhao et al., 2011). See Supplementary Text Section 1 in Supporting Information S1 for further details on BIOME4 modeling parameters.

3. Results

3.1. SST Comparison

We compare proxy SST reconstructions with a fitted Gaussian curve to the multi-model mean 400 and 840 ppm middle Miocene MioMIP1 simulations published in Burls et al. (2021), and the fully coupled versions of the Mio400, Mio840, and Preindustrial (PI) simulations published in Acosta et al. (2022) and Gaskell et al. (2022) (Figure 1a). We find the reconstructed mean tropical SSTs (10°S to 10°N) and the 400 ppm simulations are 1–5°C warmer than the PI simulation, while the 840 ppm simulations being 8–10°C warmer than the PI simulation (Figure 1a). In the Southern Hemisphere, much of the reconstructed SSTs reside within the range of the Mio400 and Mio840 simulations and are warmer than PI. In the Northern Hemisphere, models tend to underestimate the mid-and high latitudes temperatures and thereby the equator-to-pole temperature gradient (Figures 1a and 1c).

3.2. European and Northern Africa Climate During the MCO

In both Mio400 and Mio840, the wettest region of Europe is over northern Europe (900–1,500 mm), while the driest regions are found over southern Europe and the Mediterranean (300–700 mm). The Mio840 has a higher MAP (Figures 2a and 2b) and seasonal precipitation (Figures S4 and S5 in Supporting Information S1) over northern Europe than the Mio400, but overall has the same precipitation patterns. Regardless, both simulations underestimate the high MAP derived from paleobotanical proxies, but overestimate rainfall compared to herpetological evidence (Figures 2a and 2b). Over Northern Africa, both Mio400 and Mio840 show dry conditions with MAP ranging between 0 and 200 mm. The regional bias analysis shows the Mio400 and Mio840 cases have a RMSB of ∼350 and ∼352 mm against the paleobotanical records from MioMIP1, ∼153 and ∼141 mm against the herpetological records, and ∼221 and ∼238 mm against the newly added paleobotanical data set. The RMSB analysis suggests both Mio400 and Mio840 cases compare better with the herpetological than the paleobotanical evidence. Pointwise bias comparison is provided in the Supplementary Figure S2 in Supporting Information S1.

The Mio400.NAZM simulation maintains wet conditions in northern Europe, and increase rainfall over the Mediterranean regions which better match the paleobotanical evidence (Figure 2c). In this simulation, parts of southwestern Europe maintain the low precipitation corridor where a majority of the herpetological evidence resides and are potentially impacted by topography and rain shadow effects. Northern Africa is substantially wetter in the Mio400.NAZM than the Mio400 and Mio840 cases. The regional bias analysis shows the Mio400.NAZM case compares well with the MioMIP1 paleobotanical evidence with the RMSB of ∼90 mm. However, the Mio400.NAZM case does poorly against the herpetological records with an RMSB of ∼242 mm. Comparison against the newly added paleobotanical data set the Mio400.NAZM simulation has a low RMSB of ∼117 mm.

When considering temperature reconstructions, increasing CO_2 between the Mio400 to the Mio840 and adding warmer North Atlantic SSTs increases MAT over land (Figures 2d and 2f). The regional bias analysis against the MioMIP1 paleobotanical records shows Mio400, Mio840, and Mio400.NAZM have an RMSB of ∼2°C. Compared to the new paleobotanical data set, the Mio400 (∼5°C) has a lower RMSB than the Mio840 and the Mio400.NAZM (∼7°C). For seasonal temperature comparison between simulations see Figures S6 and S7 in Supporting Information S1. The difference in RMSBs between the simulations is due to the increased number of sites near the Mediterranean coast much warmer than the new paleobotanical data set (Figure S2 in Supporting Information S1).

3.3. Role of IVTs and Surface Evaporation on MAP

The warmer North Atlantic and Mediterranean-Tethys SSTs enhance moisture transport toward Europe (Figure 3a vs. Figures 3b and 3c). During boreal winter, IVTs are weaker over northern and central Europe in the Mio400.NAZM simulation, but are compensated by enhanced evaporation and transport of moisture from the Mediterranean-Tethys (Figure 3d, Figures S3, S8, and S10 in Supporting Information S1). Stronger IVTs occur during the boreal summer in Mio400.NAZM due to the enhancement of surface evaporation over the warmer North Atlantic and Mediterranean Sea (Figure 3e and Figure S3 in Supporting Information S1).

Increase IVT over Northern Africa under Mio400.NAZM occurs during boreal summer months, with IVTs originating from the Mediterranean-Tethys Sea (Figure 3e, Figures S3, S9, and S10 in Supporting Information S1). The increase onshore transport toward the region supplies moisture for the North African monsoon (Figure S10 in Supporting Information S1). Small differences in IVTs and evaporation rates occur over Northern

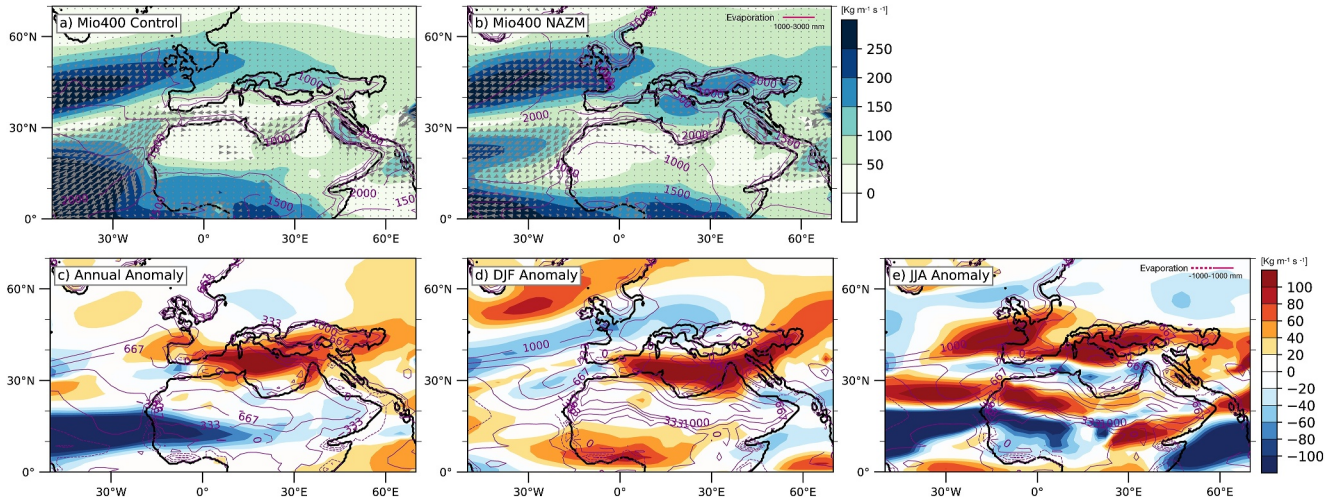

Figure 3. Column integrated total water vapor transport (1,000–1,300 mb) analysis overlain with mean surface evaporation (purple contours). Annual, boreal summer, and boreal winter comparison between Mio400 (control) and Mio400.NAZM is shown.

Africa during winter (Figure 3d), suggesting most of the annual mean signal occurs during the boreal summer months when the North African monsoon is active (Figure 3e and Figure S3 in Supporting Information S1).

3.4. Vegetation Type

BIOME4 driven by our simulated atmospheric fields predicts the presence of temperate forests across central Europe in all cases (Figure 4). However, the paleobotanical data reconstructs warm-temperature mixed forests between 40 and 50°N, which is only modeled when BIOME4 is driven by the Mio840 and Mio400.NAZM simulations. Shrubland biomes along southwestern Europe is only simulated when BIOME4 is driven by the Mio400 climate simulation which indicate dry coastal regions. Increased CO_2 or SSTs, enable tropical deciduous forests to emerge along the northern Mediterranean Sea coastline, depicting a warmer temperate mixed forest biome (McCoy et al., 2022). New paleobotanical data from Northern Africa suggests the presence of a tropical deciduous forest biome at ~30°N and ~30°E as well as more warm temperate mixed forest biomes. Northern Africa in the Mio400 and Mio840 simulations composed of shrubland, savanna, and patches of tropical forest biomes potentially indicate some heavy seasonal rainfall but with distinct dry seasons. The presence of an expanded tropical deciduous forest is only simulated when BIOME4 is driven by the Mio400.NAZM climate simulations indicate substantially more seasonal rainfall but with persistent year-round rainfall (Figure S4 in Supporting Information S1).

4. Discussion

There are conflicting MCO climate signals between herpetological and paleobotanical records, which represents an important hydroclimate conundrum. Analysis from a recent Europe-specific study (Botsyun et al., 2022) shows paleoclimate simulations reproduce a drier European climate during the MCO. Drying of the subtropics and Mediterranean regions is aligned with the theory of poleward expansion of subtropical dry zones under warming conditions (Langenbrunner et al., 2015; Doblas-Reyes et al., 2021; Douville et al., 2021). However, changes in SST patterns (Burls & Fedorov, 2017; Dittus et al., 2024) have been shown to influence regional climate. Here, we demonstrated that the inability of MioMIP1 simulations to capture the North Atlantic SST reconstructions is a key contributor to the low MioMIP1 MAP model-data agreement with paleobotanical data.

Our findings are in contrast with linearly increasing CO_2 concentrations resulting in continuous drying of the Mediterranean and North African region during the MCO (e.g., Mio400 to Mio840 simulations). Under an alternative equilibrium state, where a warmer North Atlantic SST distribution is maintained (Dittus et al., 2024), the enhancement of local evaporation and strengthening of IVTs increases MAP over Europe (Figures S10 and S11 in Supporting Information S1). Additionally, capturing warmer North Atlantic, Mediterranean and Paratethys Seas also results in the enhancement of the North African Monsoon. We note that aside from changes in SST, a

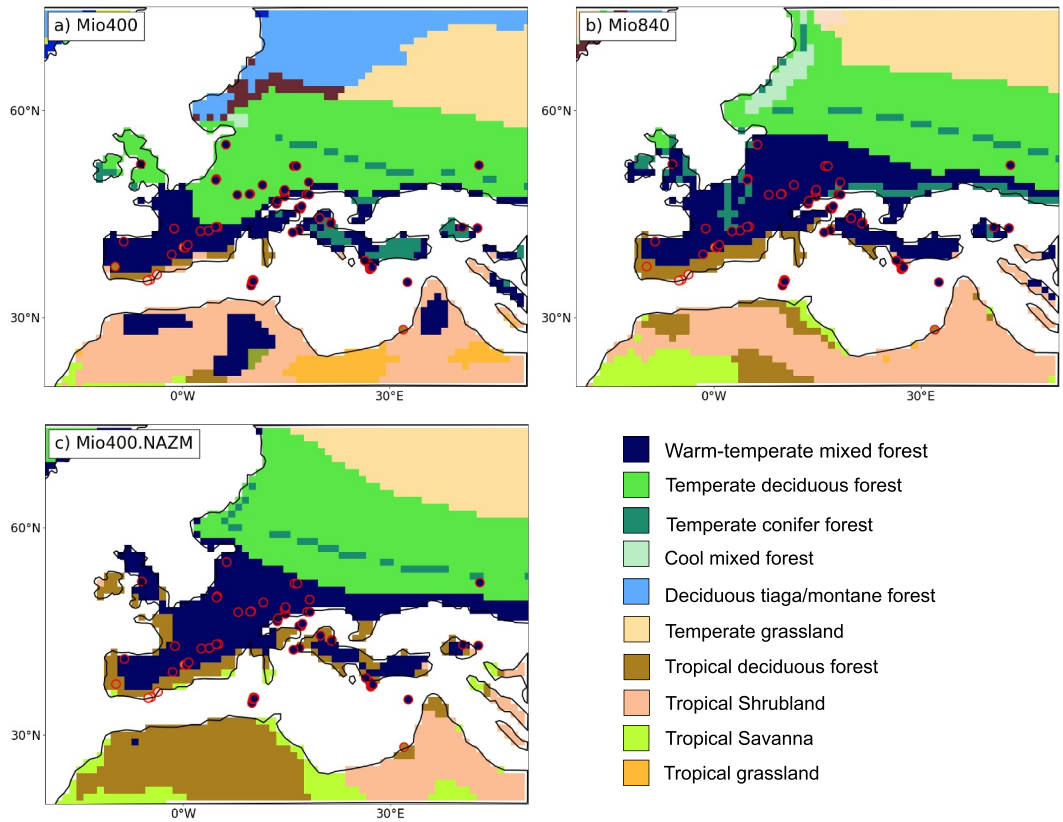

Figure 4. Results from BIOME4 analysis. Scenarios were forced with temperature, precipitation, and solar insolation from Mio400, Mio840, and Mio400.NAZM simulations.

key feature of our simulations, is the Tethyan-Indian Ocean gateway, which has been found to reduce in size and close during the Neogene (Harzhauser & Piller, 2007; Hamon et al., 2013; Straume et al., 2024). Albeit its timing is still debated, its closure has been shown to change SST patterns (Hamon et al., 2013) and lead to regional drying patterns (Zhang et al., 2014).

The opposing regional signals between herpetological and paleobotanical evidence are difficult to reconcile, and the increased regional MAP under Mio400.NAZM simulation also increases model-data bias with the herpetological records. We find further confining our regional analysis should yield reduced model-data bias compared to herpetological records. For example, a limited number of herpetological records from central eastern Europe show MAP above 1,000 mm, which are comparable to both the paleobotanical evidence and the Mio400.NAZM simulation (MAP 1,000–1,500 mm; Figure S12 in Supporting Information S1). Meanwhile, evidence from sediments and mammal assemblages (van Dam, 2006; Retallack, 2022) supports a dry southwest Europe, which has the lowest modeled rainfall in the region. Additionally, we found majority of the herpetological evidence resides in regions of variable topography (Krsnik et al., 2021; Boateng et al., 2022), which impacts model-data comparison (Acosta et al., 2023; Figure S12 in Supporting Information S1). Here, we demonstrate that our Mio400.NAZM simulation maintains a relatively dry corridor along the mountain range, but is potentially unable to further resolve critical dry zones due to orographic effects requiring higher spatial modeling resolution (Acosta & Huber, 2017; Botsyun et al., 2022).

The simulated mixed forest and tropical rainforest landscape over Europe and Northern Africa under the Mio400.NAZM simulation is supported by previous studies (Morley, 2011; Polissar et al., 2019; Gibson et al., 2022; McCoy et al., 2022) and paleobotanical records presented in our study. We note that although Europe was initialized with boreal forest and shrubland biome, while Northern Africa with a temperate forest in our simulations, increased CO_2 can override the required MAP and MAT for such vegetation change and continue to produce much drier biomes. Here we emphasize changes in ocean circulation and in particular SST patterns (Burls

& Fedorov, 2017; Dittus et al., 2024) as a mechanism that maintains a humid biome over Europe and Northern Africa during the MCO.

We acknowledge the uncertainties associated with our idealized SST simulations. The lack of samples found near Northern Hemisphere polar regions >80° N, and especially over the Pacific Ocean, could be potentially skewing our global Gaussian curve toward warmer SSTs or weaker Northern Hemisphere meridional temperature gradient. However, we argue that the extensive terrestrial records presented in our study can be used as an independent constrain on the regional SST records. Nonetheless, the key mechanism driving such warm SSTs over the North Atlantic remains unknown. Changes in the Atlantic Meridional Overturning Circulation through its response to CO_2 change (Orihuela-Pinto et al., 2022; Dittus et al., 2024), opening of Arctic gateways (Stärz et al., 2017; Hossain et al., 2021; Weiffenbach et al., 2023; Liu et al., 2024), or regional cloud radiative feedbacks (Yuan et al., 2016; Menary et al., 2020) are potential culpable forcings. Despite poor constraints on mechanisms, modification of North Atlantic and Mediterranean SST distribution that is in accordance with current best SST proxy-based estimates are much warmer than modern-day, suggesting that typical paleoclimate models are unable to capture such a key process over the North Atlantic during the MCO.

5. Conclusion

This study presented a suite of CESM1.2 middle Miocene simulations with multiple European and Northern African climate scenarios. We demonstrate that the implementation of proxy-based North Atlantic and Mediterranean SST patterns that capture the extreme mid-latitude warmth seen in the proxy reconstructions enable middle Miocene simulations to produce paleobotanical MAP reconstructions over Europe and Northern Africa. A strengthening of IVTs in response to enhanced North Atlantic evaporation produces a wetter European climate, while the strengthening of the North African Monsoon produces a wetter North Africa. Vegetation model analysis supports much wetter European and Northern African environments that are conducive to a forested paleoenvironment. Findings from this work highlight the potential deviation of Mediterranean hydroclimate from theoretical drying should the adjacent ocean experience amplified warming.

Data Availability Statement

Proxy synthesis and output for MCO simulations used for Miocene model-data comparison can be found in Zenodo repository (Acosta et al., 2024) for peer review.

Acknowledgments

R. P. Acosta and N. J. Burls acknowledge support from NSF AGS-1844380, and NSF EAR-2303417. M. J. Pound, M. Gibson, and J. McCoy acknowledge support from NERC grant NE/V01501X/1 and Royal Society IECR2202086. C. D. Bradshaw acknowledges NERC Grant NE/I006281/1 and a NERC PhD studentship. S.J. Feakins acknowledges support from NSF EAR-2303418. J. M. K. O'Keefe acknowledges NSF GEO-2015813. We thank NCAR CISL Data Support section and Glade (NSFEAR114504) for maintaining and facilitating interactive computing JupyterHub, which we utilize to postprocess our data. The authors thank N. Herold for the valuable discussion on the model experiment design and the reviewers for their thoughtful suggestions.

References

Acosta, R. P., Burls, N., Pound, M., Bradshaw, C., McCoy, J., Gibson, M., et al. (2024). Climate conundrum: A wet or dry European and northern African climate during the middle miocene [Dataset]. https://doi.org/10.5281/zenodo.13524475

Acosta, R. P., Burls, N. J., Pound, M. J., Bradshaw, C. D., De Boer, A. M., Herold, N., et al. (2023). A model-data comparison of the hydrological response to miocene warmth: Leveraging the MioMIP1 opportunistic multi-model ensemble. *Paleoceanography and Paleoclimatology*, *39*(e2023PA004726), 1–29. https://doi.org/10.1029/2023PA004726

Acosta, R. P., & Huber, M. (2017). The neglected Indo-Gangetic Plains low-level jet and its importance for moisture transport and precipitation during the peak summer monsoon. *Geophysical Research Letters*, *44*(16), 8601–8610. https://doi.org/10.1002/2017GL074440

Acosta, R. P., & Huber, M. (2020). Competing topographic mechanisms for the summer Indo-Asian monsoon. *Geophysical Research Letters*, *47*(3). https://doi.org/10.1029/2019GL085112

Acosta, R. P., Ladant, J.-B., Zhu, J., & Poulsen, C. J. (2022). Evolution of the Atlantic intertropical convergence zone, and the South American and African monsoons over the past 95-Myr and their impact on the tropical rainforests. *Paleoceanography and Paleoclimatology*, *37*(7), e2021PA004383. https://doi.org/10.1029/2021PA004383

Boateng, D., Mutz, S. G., Ballian, A., Meijers, M. J. M., Methner, K., Botsyun, S., et al. (2022). The effects of diachronous surface uplift of the European Alps on regional climate and the oxygen isotopic composition of precipitation, (December) (pp. 1–45).

Böhme, M., Ilg, A., Ossig, A., & Küchenhoff, H. (2006). New method to estimate paleoprecipitation using fossil amphibians and reptiles and the middle and late Miocene precipitation gradients in Europe. *Geology*, *34*(6), 425–428. https://doi.org/10.1130/G22460.1

Böhme, M., Winklhofer, M., & Ilg, A. (2011). Miocene precipitation in Europe: Temporal trends and spatial gradients. *Palaeogeography, Palaeoclimatology, Palaeoecology*, *304*(3–4), 212–218. https://doi.org/10.1016/j.palaeo.2010.09.028

Botsyun, S., Ehlers, T. A., Koptev, A., Risi, C., Stepanek, C., Mutz, S. G., et al. (2022). Middle Miocene climate and stable oxygen isotopes in Europe based on numerical modeling. *Paleoceanography and Paleoclimatology*, *37*(10), 1–42. https://doi.org/10.1029/2022PA004442

Bradshaw, C. D., Lunt, D. J., Flecker, R., & Davies-Barnard, T. (2015). Disentangling the roles of late Miocene palaeogeography and vegetation - implications for climate sensitivity. *Palaeogeography, Palaeoclimatology, Palaeoecology*, *417*, 17–34. https://doi.org/10.1016/j.palaeo.2014.10.003

Bruch, A. A., Uhl, D., & Mosbrugger, V. (2007). Miocene climate in Europe - patterns and evolution. A first synthesis of NECLIME. *Palaeogeography, Palaeoclimatology, Palaeoecology*, *253*(1–2), 1–7. https://doi.org/10.1016/j.palaeo.2007.03.030

Burls, N. J., Bradshaw, C. D., De Boer, A. M., Herold, N., Huber, M., Pound, M., et al. (2021). Simulating miocene warmth: Insights from an opportunistic multi-model ensemble (MioMIP1). *Paleoceanography and Paleoclimatology*, *36*(5). https://doi.org/10.1029/2020pa004054

Burls, N. J., & Fedorov, A. V. (2017). Wetter subtropics in a warmer world: Contrasting past and future hydrological cycles. *Proceedings of the National Academy of Sciences of the United States of America*, *114*(49), 12888–12893. https://doi.org/10.1073/pnas.1703421114

Dittus, A. J., Collins, M., Sutton, R., & Hawkins, E. (2024). Reversal of projected European summer precipitation decline in a stabilizing climate. *Geophysical Research Letters*, *51*(6). https://doi.org/10.1029/2023GL107448

Doblas-Reyes, F. J., Sörensson, A. A., Almazroui, M., Dosio, A., Gutowski, W. J., Aðalgeirsdóttir, G., et al. (2021). Linking global to regional climate change.

Douville, H., Raghavan, K., & Renwick, J. (2021). Water cycle changes. *Clim. Chang. 2021 Phys. Sci. Basis. Contrib. Work. Gr. I to Sixth Assess. Rep. IPCC*, 1055–1210. https://doi.org/10.1017/9781009157896.010.1055

Foster, G. L., Lear, C. H., & Rae, J. W. B. (2012). The evolution of pCO 2, ice volume and climate during the middle Miocene. *Earth and Planetary Science Letters*, *341–344*, 243–254. https://doi.org/10.1016/j.epsl.2012.06.007

Gaskell, D. E., Huber, M., O'Brien, C. L., Inglis, G. N., Acosta, R. P., Poulsen, C. J., & Hull, P. M. (2022). The latitudinal temperature gradient and its climate dependence as inferred from foraminiferal δ18O over the past 95 million years. *Proceedings of the National Academy of Sciences*, *119*(11), 1–8. https://doi.org/10.1073/pnas.2111332119/-/DCSupplemental.Published

Geen, R., Bordoni, S., Battisti, D. S., & Hui, K. (2020). Monsoons, ITCZs and the concept of the global monsoon. *Reviews of Geophysics*, *58*(4), 1–45. https://doi.org/10.1029/2020rg000700

Gibson, M. E., McCoy, J., O'Keefe, J. M. K., Otaño, N. B. N., Warny, S., & Pound, M. J. (2022). Reconstructing terrestrial paleoclimates: A comparison of the Co-existence approach, Bayesian and probability reconstruction techniques using the UK Neogene. *Paleoceanography and Paleoclimatology*, *37*(2), 1–18. https://doi.org/10.1029/2021PA004358

Gulev, S. K., & Thorne, P. W. (2021). The changing state of the climate. *Clim. Chang. 2021 Phys. Sci. Basis. Contrib. Work. Gr. I to Sixth Assess. Rep. Intergov. Panel Clim. Chang.*, 1–4. https://doi.org/10.1017/9781009157896.004.288

Hamon, N., Sepulchre, P., Lefebvre, V., & Ramstein, G. (2013). The role of eastern tethys seaway closure in the middle miocene climatic transition (ca. 14 Ma). *Climate of the Past*, *9*(6), 2687–2702. https://doi.org/10.5194/cp-9-2687-2013

Harrison, S. P., & Prentice, C. I. (2003). Climate and CO2 controls on global vegetation distribution at the last glacial maximum: Analysis based on palaeovegetation data, biome modelling and palaeoclimate simulations. *Global Change Biology*, *9*(7), 983–1004. https://doi.org/10.1046/j.1365-2486.2003.00640.x

Harzhauser, M., & Piller, W. E. (2007). Benchmark data of a changing sea - palaeogeography, palaeobiogeography and events in the central Paratethys during the miocene. *Palaeogeography, Palaeoclimatology, Palaeoecology*, *253*(1–2), 8–31. https://doi.org/10.1016/j.palaeo.2007.03.031

Herbert, T. D., Lawrence, K. T., Tzanova, A., Peterson, L. C., Caballero-Gill, R., & Kelly, C. S. (2016). Late Miocene global cooling and the rise of modern ecosystems. *Nature Geoscience*, *9*(11), 843–847. https://doi.org/10.1038/ngeo2813

Herold, N., Müller, R. D., & Seton, M. (2010). Comparing early to middle Miocene terrestrial climate simulations with geological data. *Geosphere*, *6*(6), 952–961. https://doi.org/10.1130/ges00544.1

Hossain, A., Knorr, G., Jokat, W., & Lohmann, G. (2021). Opening of the fram strait led to the establishment of a modern-like three-layer stratification in the Arctic ocean during the miocene. *Arktos*, *7*(1–3), 1–12. https://doi.org/10.1007/s41063-020-00079-8

Jackson, L. C., Kahana, R., Graham, T., Ringer, M. A., Woollings, T., Mecking, J. V., & Wood, R. A. (2015). Global and European climate impacts of a slowdown of the AMOC in a high resolution GCM. *Climate Dynamics*, *45*(11–12), 3299–3316. https://doi.org/10.1007/s00382-015-2540-2

Kaplan, J. O., Bigelow, N. H., Prentice, I. C., Harrison, S. P., Bartlein, P. J., Christensen, T. R., et al. (2003). Climate change and Arctic ecosystems: 2. Modeling, paleodata-model comparisons, and future projections. *Journal of Geophysical Research*, *108*(19). https://doi.org/10.1029/2002jd002559

Krsnik, E., Methner, K., Campani, M., Botsyun, S., Mutz, S. G., Ehlers, T. A., et al. (2021). Miocene high elevation in the central Alps. *Solid Earth*, *12*(11), 2615–2631. https://doi.org/10.5194/se-12-2615-2021

Langenbrunner, B., Neelin, J. D., Lintner, B. R., & Anderson, B. T. (2015). Patterns of precipitation change and climatological uncertainty among CMIP5 models, with a focus on the midlatitude pacific storm track. *Journal of Climate*, *28*(19), 7857–7872. https://doi.org/10.1175/JCLI-D-14-00800.1

Lavers, D. A., & Villarini, G. (2013). The nexus between atmospheric rivers and extreme precipitation across Europe. *Geophysical Research Letters*, *40*(12), 3259–3264. https://doi.org/10.1002/grl.50636

Lavers, D. A., & Villarini, G. (2015). The relationship between daily European precipitation and measures of atmospheric water vapour transport. *International Journal of Climatology*, *35*(8), 2187–2192. https://doi.org/10.1002/joc.4119

Liu, X., Herold, N., & Huber, M. (2024). Atlantic meridional overturning circulation influence on the annual mean intertropical convergence zone location in the miocene. *Geophysical Research Letters*, *51*(9). https://doi.org/10.1029/2024GL109159

Matthews, K. J., Maloney, K. T., Zahirovic, S., Williams, S. E., Seton, M., & Müller, R. D. (2016). Global plate boundary evolution and kinematics since the late Paleozoic. *Global and Planetary Change*, *146*, 226–250. https://doi.org/10.1016/j.gloplacha.2016.10.002

McCoy, J., Barrass-Barker, T., Hocking, E. P., O'Keefe, J. M. K., Riding, J. B., & Pound, M. J. (2022). Middle Miocene (Serravallian) wetland development on the northwest edge of Europe based on palynological analysis of the uppermost Brassington Formation of Derbyshire, United Kingdom. *Palaeogeography, Palaeoclimatology, Palaeoecology*, *603*(August), 111180. https://doi.org/10.1016/j.palaeo.2022.111180

Meehl, G. a., Washington, W. M., Arblaster, J. M., Hu, A., Teng, H., Kay, J. E., et al. (2013). Climate change projections in CESM1(CAM5) compared to CCSM4. *Journal of Climate*, *26*(17), 6287–6308. https://doi.org/10.1175/JCLI-D-12-00572.1

Menary, M. B., Robson, J., Allan, R. P., Booth, B. B. B., Cassou, C., Gastineau, G., et al. (2020). Aerosol-forced AMOC changes in CMIP6 historical simulations. *Geophysical Research Letters*, *47*(14). https://doi.org/10.1029/2020GL088166

Morley, R. J. (2011). Cretaceous and Tertiary climate change and the past distribution of megathermal rainforests. In M. Bush, J. Flenley, & W. Gosling (Eds.), *Tropical rainforest responses to climatic change* (pp. 1–34). Springer Berlin Heidelberg.

Müller, R. D., Cannon, J., Qin, X., Watson, R. J., Gurnis, M., Williams, S., et al. (2018). GPlates: Building a virtual Earth through Deep time. *Geochemistry, Geophysics, Geosystems*, *19*(7), 2243–2261. https://doi.org/10.1029/2018GC007584

Ni, J., & Herzschuh, U. (2011). Simulating biome distribution on the Tibetan Plateau using a modified global vegetation model. *Arctic Antarctic and Alpine Research*, *43*(3), 429–441. https://doi.org/10.1657/1938-4246-43.3.429

Orihuela-Pinto, B., England, M. H., & Taschetto, A. S. (2022). Interbasin and interhemispheric impacts of a collapsed Atlantic overturning circulation. *Nature Climate Change*, *12*(6), 558–565. https://doi.org/10.1038/s41558-022-01380-y

Payne, A. E., Demory, M. E., Leung, L. R., Ramos, A. M., Shields, C. A., Rutz, J. J., et al. (2020). Responses and impacts of atmospheric rivers to climate change. *Nature Reviews Earth & Environment*, *1*(3), 143–157. https://doi.org/10.1038/s43017-020-0030-5

Polissar, P. J., Rose, C., Uno, K. T., Phelps, S. R., & de Menocal, P. (2019). Synchronous rise of African C4 ecosystems 10 million years ago in the absence of aridification. *Nature Geoscience*, *12*(8), 657–660. https://doi.org/10.1038/s41561-019-0399-2

Pound, M. J., Haywood, A. M., Salzmann, U., & Riding, J. B. (2012). Global vegetation dynamics and latitudinal temperature gradients during the Mid to Late Miocene (15.97-5.33Ma). *Earth-Science Reviews*, *112*(1–2), 1–22. https://doi.org/10.1016/j.earscirev.2012.02.005

Pound, M. J., Tindall, J., Pickering, S. J., Haywood, A. M., Dowsett, H. J., & Salzmann, U. (2014). Late pliocene lakes and soils: A global data set for the analysis of climate feedbacks in a warmer world. *Climate of the Past*, *10*(1), 167–180. https://doi.org/10.5194/cp-10-167-2014

Rae, J. W. B., Zhang, Y. G., Liu, X., Foster, G. L., Stoll, H. M., & Whiteford, R. D. M. (2021). Atmospheric CO2 over the past 66 million years from marine archives. *Annual Review of Earth and Planetary Sciences*, *49*(1), 609–641. https://doi.org/10.1146/annurev-earth-082420-063026

Retallack, G. J. (2022). Soil carbon dioxide planetary thermostat. *Astrobiology*, *22*(1), 116–123. https://doi.org/10.1089/ast.2020.2415

Salzmann, U., Haywood, A. M., Lunt, D. J., Valdes, P. J., & Hill, D. J. (2008). A new global biome reconstruction and data-model comparison for the Middle Pliocene. *Global Ecology and Biogeography*, *17*(3), 432–447. https://doi.org/10.1111/j.1466-8238.2008.00381.x

Sosdian, S. M., Babila, T. L., Greenop, R., Foster, G. L., & Lear, C. H. (2020). Ocean carbon storage across the middle miocene: A new interpretation for the monterey event. *Nature Communications*, *11*(1), 1–11. https://doi.org/10.1038/s41467-019-13792-0

Spicer, R. A., Yang, J., Spicer, T. E. V., & Farnsworth, A. (2021). Woody dicot leaf traits as a palaeoclimate proxy: 100 years of development and application. *Palaeogeography, Palaeoclimatology, Palaeoecology*, *562*(September 2020), 110138. https://doi.org/10.1016/j.palaeo.2020.110138

Stärz, M., Jokat, W., Knorr, G., & Lohmann, G. (2017). Threshold in North Atlantic-Arctic ocean circulation controlled by the subsidence of the Greenland-Scotland ridge. *Nature Communications*, *8*, 1–13. https://doi.org/10.1038/ncomms15681

Straume, E. O., Steinberger, B., Becker, T. W., & Faccenna, C. (2024). Impact of mantle convection and dynamic topography on the cenozoic paleogeography of central Eurasia and the west Siberian seaway. *Earth and Planetary Science Letters*, *630*(January), 118615. https://doi.org/10.1016/j.epsl.2024.118615

Super, J. R., Thomas, E., Pagani, M., Huber, M., O'Brien, C., & Hull, P. M. (2018). North Atlantic temperature and pCO2 coupling in the early-middle Miocene. *Geology*, *46*(6), 519–522. https://doi.org/10.1130/G40228.1

Super, J. R., Thomas, E., Pagani, M., Huber, M., O'Brien, C. L., & Hull, P. M. (2020). Miocene evolution of North Atlantic sea surface temperature. *Paleoceanography and Paleoclimatology*, *35*(5), 1–15. https://doi.org/10.1029/2019PA003748

Ukkola, A. M., De Kauwe, M. G., Roderick, M. L., Abramowitz, G., & Pitman, A. J. (2020). Robust future changes in meteorological drought in CMIP6 projections despite uncertainty in precipitation. *Geophysical Research Letters*, *47*(11), 1–9. https://doi.org/10.1029/2020GL087820

Utescher, T., Bruch, A. A., Erdei, B., François, L., Ivanov, D., Jacques, F. M. B., et al. (2014). The Coexistence Approach-Theoretical background and practical considerations of using plant fossils for climate quantification. *Palaeogeography, Palaeoclimatology, Palaeoecology*, *410*, 58–73. https://doi.org/10.1016/j.palaeo.2014.05.031

van Dam, J. A. (2006). Geographic and temporal patterns in the late Neogene (12-3 Ma) aridification of Europe: The use of small mammals as paleoprecipitation proxies. *Palaeogeography, Palaeoclimatology, Palaeoecology*, *238*(1–4), 190–218. https://doi.org/10.1016/j.palaeo.2006.03.025

Wang, S., Ma, X., Zhou, S., Wu, L., Wang, H., Tang, Z., et al. (2023). Extreme atmospheric rivers in a warming climate. *Nature Communications*, *14*(1), 3219. https://doi.org/10.1038/s41467-023-38980-x

Weiffenbach, J. E., Baatsen, M. L. J., Dijkstra, H. A., Von Der Heydt, A. S., Abe-Ouchi, A., Brady, E. C., et al. (2023). Unraveling the mechanisms and implications of a stronger mid-pliocene Atlantic meridional overturning circulation (AMOC) in PlioMIP2. *Climate of the Past*, *19*(1), 61–85. https://doi.org/10.5194/cp-19-61-2023

Westerhold, T., Marwan, N., Drury, A. J., Liebrand, D., Agnini, C., Anagnostou, E., et al. (2020). An astronomically dated record of Earth's climate and its predictability over the last 66 million years. *Science (80-.)*, *369*(6509), 1383–1388. https://doi.org/10.1126/SCIENCE.ABA6853

Yuan, T., Oreopoulos, L., Zelinka, M., Yu, H., Norris, J. R., Chin, M., et al. (2016). Positive low cloud and dust feedbacks amplify tropical North Atlantic Multidecadal Oscillation. *Geophysical Research Letters*, *43*(3), 1349–1356. https://doi.org/10.1002/2016GL067679

Zhang, Z., Ramstein, G., Schuster, M., Li, C., Contoux, C., & Yan, Q. (2014). Aridification of the Sahara desert caused by Tethys Sea shrinkage during the late miocene. *Nature*, *513*(7518), 401–404. https://doi.org/10.1038/nature13705

Zhao, D., Wu, S., Yin, Y., & Yin, Z. Y. (2011). Vegetation distribution on Tibetan Plateau under climate change scenario. *Regional Environmental Change*, *11*(4), 905–915. https://doi.org/10.1007/s10113-011-0228-7